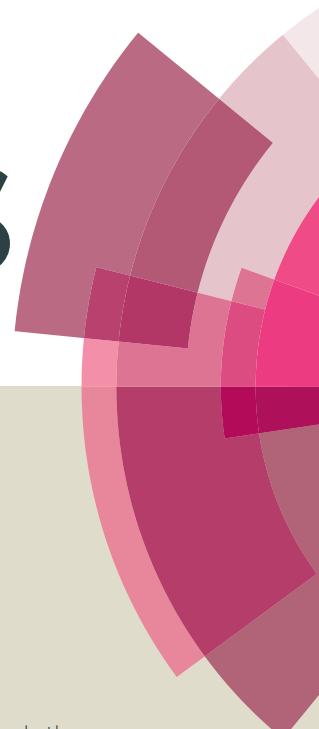


RSC Advances



This article can be cited before page numbers have been issued, to do this please use: M. Das, F. Baig and M. Sarkar, *RSC Adv.*, 2016, DOI: 10.1039/C6RA08582B.



This is an *Accepted Manuscript*, which has been through the Royal Society of Chemistry peer review process and has been accepted for publication.

Accepted Manuscripts are published online shortly after acceptance, before technical editing, formatting and proof reading. Using this free service, authors can make their results available to the community, in citable form, before we publish the edited article. This *Accepted Manuscript* will be replaced by the edited, formatted and paginated article as soon as this is available.

You can find more information about *Accepted Manuscripts* in the [Information for Authors](#).

Please note that technical editing may introduce minor changes to the text and/or graphics, which may alter content. The journal's standard [Terms & Conditions](#) and the [Ethical guidelines](#) still apply. In no event shall the Royal Society of Chemistry be held responsible for any errors or omissions in this *Accepted Manuscript* or any consequences arising from the use of any information it contains.

Cite this: DOI: 10.1039/c0xx00000x

www.rsc.org/xxxxxx

ARTICLE TYPE

Photo Physical Properties of Di-Schiff Bases: Evaluating the Synergistic Effect of Non Covalent Interactions and Alkyl Spacer in Enhanced Emissions of Solids

Moyna Das, Fayaz Baig and Madhushree Sarkar*

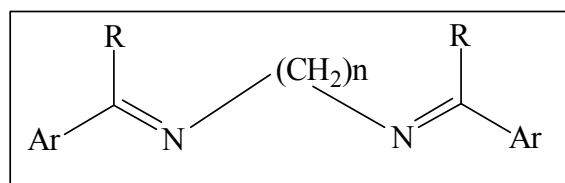
Received (in XXX, XXX) Xth XXXXXXXXX 20XX, Accepted Xth XXXXXXXXX 20XX
DOI: 10.1039/b000000x

Photo physical properties of di-Schiff base compounds in the solution and solid states are explored. The di-Schiff bases with alkyl spacer (ethyl, butyl and hexyl) showed enhanced light emitting properties in solid state, while quenching was observed for di-Schiff bases with hydrazine spacer. The photoluminescence spectra and the crystal structure were compared with *bis*-pyridyl-ethyl-di-imine and *bis*-pyridyl-butyl-di-imine. The crystal structure analysis of the compounds rationalizes the observed results. The concentration dependent ¹H-NMR and NOESY spectra showed the aggregation behaviour of the

Introduction

The potential application¹ of light emitting materials includes organic light-emitting diodes (OLEDs), sensors and biological imaging, which requires them to have enhanced luminescence efficiency in the aggregated state. Tang and coworkers in 2001 first explored the aggregation based emission (AIE) and reported a series of tetraphenylethene derivatives.² Park and co-workers³, Tian and co workers⁴ have reported several material systems with AIE properties. The AIE behavior is rationalized by considering the restriction of Intramolecular Rotation, formation of J-aggregates and intramolecular planarization.⁵ The solid state arrangement of the molecules, in general, decides the properties of a compound, so the crystal structure analysis will provide information on arrangement of the molecules. The knowledge on supramolecular packing of the molecules and its relation with the photophysical property will pave the way to develop the strategies to design new materials targeting the light emitting properties. The synthesis of materials by utilizing non covalent interaction is an efficient route and is a handy method to tailor made light emitting solids. Draper and co workers have used supramolecular synthesis and tuned the solid state luminescence of 2-cyano-3(4-(diphenylamino)phenyl)acrylic acid by reacting them with substituted pyridines and amines.⁶ The review on non-covalent methods to synthesize solid state emitting molecular materials and their applications is highlighted by Varughese.⁷ The Schiff Base based compounds are explored widely because of their easy synthetic procedures, photophysical properties and biological activity.⁸ Kawasaki *et al.* have reported the solid state PL spectra for a series of Salen compounds (Schiff Bases) with varying alkyl chain length. They have observed a relation of photo physical property with the alkyl chain length.⁹ Xiang *et al.* have reported AIE in salicylaldehyde azine where despite having planar geometry, no quenching was observed.¹⁰ Recently, Xiang, Liu and

coworkers have reported the non conjugated Salen compounds with unique AIE, where the small π -conjugated system resulted in aggregation-induced emission (AIE) with large Stokes shifts and high fluorescence quantum yields was observed.^{10e} In the present work, we have studied the photophysical properties of di Schiff base molecules (Scheme 1) in the solid state and in solution. We have rationalized the observations on the following grounds: (i) Effect of alkyl chain length; (ii) Presence of methyl group on the methinine carbon; (iii) Comparison of the light emitting properties with the pyridyl based Schiff base compounds. Recently our group has reported the photo physical properties along with the structural description of pyridyl based Schiff bases, where we have concluded that the flexible spacer (alkyl bridge) in these molecules helped in aggregating the molecules which results in enhanced emission.¹¹



n = 0: **L1**
= 2: **L2**
= 4: **L3**
= 6: **L4**

Ar = phenyl and R = H: **a**
Ar = phenyl and R = CH₃: **b**
Ar = 2-pyridyl and R = H: **c**
Ar = 2-pyridyl and R = CH₃: **d**

Scheme 1: Di Schiff Base Compounds

There are reports on the crystal structure analysis of **L1a**, **L1b** and **L2a** along with their property studies.¹² The absorption spectra of Azines and Dianils, which included **L1a**, **L1b**, **L2a** and **L2b**, were reported by Ferguson and Goodwin in 1949.^{12a} Sinha reported the crystal structure of **L1a** and reported the effect of conjugation on the bond lengths.^{12b} Glaser *et al.* have reported the solid state structures of series of acetophenone azines including **L1b**^{12c} while the structure of **L2b** is reported by the research group of Tiekink^{12d}. The electrochemical behavior of the acetophenone azines were studied by Workentin *et al.*, where the effect of substituents on aryl group on the electrochemical potential was studied.^{12e} Research group of Ding reported the high pressure spectral analysis of **L1a** and observed pressure induced phase transformation.^{12f} Xiang *et al.* have studied the emission properties of **L1a** and reported that no AIE properties was observed.^{10a}

Experimental Section

General: Infra Red Spectra were taken in FTIR ABB Bomen MB-3000. UV-Visible Spectra and Fluorescence Spectra were taken in Shimadzu spectrophotometer model UV-2450 and Fluorimax-4 0426C0809, respectively. Proton and Carbon-13 Nuclear Magnetic Resonance (¹H NMR and ¹³C NMR) spectra were recorded on a 400 MHz spectrophotometer (Bruker). Powder X-Ray Diffraction (XRD) were recorded with a Rigaku miniflex II, $\lambda = 1.54$, Cu K α . Fluorescence quantum yields are determined by using quanta phi instrument (Jobin Horiba, Fluoremax-4).

The compounds **L1-L4** were synthesized by the usual method of preparation of Schiff bases, which involved the condensation reaction of primary diamines with an aldehyde/ketone precursor in alcoholic solution under reflux conditions.

1,2-dibenzylidenehydrazine (L1a): Hydrazine hydrate (0.5 ml, 10 mmol.) was added drop wise to an ethanolic solution of benzaldehyde (2.0 ml, 20 mmol.). The mixture was kept for 6 hrs. under refluxing condition. The solvent was removed under vacuum and the yellow color solid product was recrystallized with methanol. Yield: 36%, Melting point: 86.5°C. IR (cm⁻¹ KBr pellet): 3418(w), 3171(w), 3047(w), 3001(w), 2947(m), 1666(m), 1628(vs), 1574(w), 489(w), 1443(m), 1304(w), 1203(w), 957(m), 856(w) (Figure S1). ¹H-NMR (400 MHz, DMSO) δ ppm: 8.73(s,1H), 7.90 (dd, $J=7.4,2.2$ Hz), 7.51 (dq, $J=6.6, 3.2$ Hz, 3H) (Figure S2). ¹³C- NMR (101 MHz DMSO) δ ppm: 161.99, 134.24, 131.84, 129.38, 128.84 (Figure S3).

1,2-bis(1-phenylethylidene)hydrazine (L1b): 0.5ml (10 mmoles) hydrazine hydrate was added dropwise to a solution of acetophenone (2.3 ml, 20 mmoles) in ethanol (40 ml). The mixture was refluxed at 80°C for 6hrs. The solvent was removed under vacuum and the yellow color solid product was recrystallized with methanol. Yield: 46%, Melting point:123°C.IR(cm⁻¹ KBr pellet): 3418(m), 3055(m), 2962(m), 2916(w), 1643(vs), 1566(vs), 1489(w), 1443(vs), 1358(vs), 1281(s), 1072(m), 1018(m), 756(vs) (Figure S4). ¹H-NMR(400 MHz, DMSO) δ ppm:7.92 (dd, $J=6.6,3.1$ Hz,2H), 7.50-7.44 (m,3H), 2.28 (s, 3H) (Figure S5).¹³C-NMR(101 MHz DMSO) δ ppm:157.77,138.77,130.54,128.79,126.80,15.19 (Figure S6).

N¹,N²-dibenzylideneethane-1,2-diamine (L2a): 0.5 ml(10mmol.) ethylene diamine was added dropwise to a solution

of benzaldehyde (2.0ml, 20 mmol.) in ethanol(40ml).The mixture was refluxed at 80°C for 6 hrs. The solvent was removed under vacuum and the orange semi-solid product was crystallized with hexane. Yield: 38%, Melting point: 60°C. IR (cm⁻¹ KBr pellet): 3418(m), 3271(w), 3055(w), 3032(w), 2908(w), 2843(m),1674(w), 1643(vs), 1574(w),1450(m), 1373(m), 1281(w), 157(w), 1018(s), 972(w), 918(w) (Figure S7). ¹H-NMR (400 MHz DMSO) δ ppm:8.34 (s,1H), 7.71 (dd, $J=7.2,2.5$ Hz, 2H), 7.48-7.36 (m,3H), 3.54-3.31 (m, 2H) (Figure S8). ¹³C-NMR(101 MHz DMSO) δ ppm:162.42,136.56,131.07,129.09,128.27,61.17 (Figure S9).

N¹,N²-bis(1-phenylethylidene)ethane-1,2-diamine(L2b): 0.5ml (10 mmol.) ethylene diamine was added dropwise to a solution of acetophenone (2.3 ml, 20 mmol.) in ethanol(40 ml).The mixture was refluxed at 80°C for 6h. The solvent was removed under vacuum and brown semi-solid product was recrystallized with hexane. Yield: 36%, Melting point: 107.5°C. IR (cm⁻¹ KBr pellet): 3418(m), 3248(w), 3063(w), 3016(w), 2885(m), 2824(m), 1628(vs), 1574(w), 1489(w), 1443(m), 1373(m), 1265(vs), 1180(w), 1080(m), 1041(m), 910(m),756(vs) (Figure S10). ¹H-NMR (400 MHz, DMSO) δ ppm: 7.92 (dd, $J = 6.6, 3.1$ Hz, 2H), 7.51 – 7.44 (m, 3H), 3.48 – 3.30 (m, 2H), 2.28 (s, 3H) (Figure S11). ¹³C-NMR (101 MHz, DMSO) δ ppm: 165.09, 140.97, 129.84, 128.45, 126.89, 52.74, 15.17 (Figure S12).

N¹,N²-dibenzylidenebutane-1,4-diamine(L3a): 0.5 ml (10mmoles) diaminobutane was added dropwise to a solution of benzaldehyde (2.0 ml, 20 mmol.) in ethanol (40ml).The mixture was refluxed at 80°C 6h. The solvent was removed under vacuum and the brown color semi-solid product was recrystallized with hexane. Yield: 49%, Melting point: 50°C. IR (cm⁻¹ KBr pellet): 3394(w), 3271(w), 3055(w), 3024(w),2932(m), 2847(m),2646(w), 1643(vs), 1605(w), 1574(w), 1443(s), 1381(w), 1288(w), 965(w),756(vs) (Figure S13). ¹ H-NMR (400 MHz, DMSO) δ ppm: 8.34 (s, 1H), 7.73 (dd, $J = 6.6, 3.1$ Hz, 2H), 7.49-7.39 (m,3H), 3.60 (d, $J = 1.1$ Hz 2H), 1.67 (Dt, $J = 5.6, 3.0$ Hz, 2H) (Figure S14).¹³C- NMR (101 MHz, DMSO) δ ppm: 161.05, 136.70, 130.96, 128.97, 128.18, 60.31, 28.58 (Figure S15).

N¹,N²-bis(1-phenylethylidene)butane-1,4-diamine(L3b): 0.5 ml (10 mmol.) diaminobutane was added dropwise to a solution of acetophenone (2.3 ml, 20 mmol.) in ethanol (40 ml). The mixture was refluxed at 80°C for 6h. The solvent was removed under vacuum and the green color semi-solid product was recrystallized with hexane. Yield: 50%, Melting point:62°C IR (cm⁻¹ KBr pellet): 3418(m), 3240(w), 3086(w),3047(w), 2932(m), 2878(m), 1628(vs), 1574(w), 1489(w), 1443(w), 1350(m), 1281(m), 1180(w), 1080(w), 918(w),764(vs) (Figure S16). ¹H-NMR (400 MHz, DMSO) δ ppm:7.82 (dd, $J=6.8,2.9$ Hz,2H),7.43-7.35 (m,3H), 3.52-3.45(m, 2H), 2.20 (s,3H), 1.84-1.75 (m, 2H) (Figure S17). ¹³C- NMR (101 MHz, DMSO) δ ppm: 163.85, 141.02, 129.73, 128.09, 127.33, 51.52, 28.98, 15.06 (Figure S18).

N¹,N²-dibenzylidenehexane-1,6-diamine (L4a): 0.5ml (10mmol.) hexamethylene diamine was added dropwise to a solution of benzaldehyde (2.0 ml,20 mmol.) in ethanol (40 ml).The mixture was refluxed at 80°C for 6h.The solvent was removed under vacuum and the brown semi-solid product was recrystallized with hexane. Yield: 48%, Melting point:170°C. IR (cm⁻¹ KBr pellet): 3394(w), 3148(m), 3001(w), 2939(w), 2854(w), 2716(w), 2106(w),1643(s),1589(w), 1551(vs), 1379(vs),

1234(w), 1173(w), 1065(w), 949(w),825(s) (Figure S19). $^1\text{H-NMR}$ (400 MHz, DMSO) δ ppm:7.89 (s, 1H), 7.44-7.23 (m, 3H), 2.70 (dd, $J = 59.6$ Hz, 2H), 1.63-1.45 (m,2H), 1.40-1.18 (m, 2H) (Figure S20). $^{13}\text{C-NMR}$ (101MHz, DMSO) δ ppm:170.46, 139.62, 129.80, 129.42, 127.83, 27.84, 25.92 (Figure S21).

N^1, N^2 -bis(1-phenylethylidene)hexane-1,6-diamine(L4b): 0.5 ml (10 mmol.) hexamethylene diamine was added dropwise to a solution of acetophenone (2.3 ml, 20 mmol.) in ethanol (40 ml).The mixture was refluxed at 80°C for 6hrs. The solvent was removed under vacuum and the brown semi-solid product was recrystallized with hexane. Yield:47%, Melting point: 47.5°C IR (cm^{-1} KBr pellet): 3811(w), 3433(m), 3256(w), 3055(w), 2924(m), 2854(w), 1628(vs), 1582(w), 1443(w), 1412(m), 1381(m), 1281(w), 794(m), 694(s),571(w) (Figure S22). $^1\text{H-NMR}$ (400 MHz, DMSO) δ ppm:7.84 – 7.76 (m, 2H), 7.45 – 7.29 (m, 3H), 3.39 (d, $J = 8.9$ Hz, 2H), 2.17 (s, 3H), 1.64 (dt, $J = 33.6, 6.9$ Hz, 2H), 1.54 – 1.27 (m, 2H) (Figure S23). $^{13}\text{C-NMR}$ (101 MHz, DMSO) δ ppm: 164.09, 141.13, 129.71, 128.26, 126.75, 51.40, 31.07, 27.55, 15.40 (Figure S24)

Results and Discussion

In order to analyze the relation of the photophysical properties of the compounds with the geometry and supramolecular arrangement of the molecules, the crystal structure description of some compounds were studied. The crystal structure of **L1a**^{12b}, **L1b**^{12c}, **L2b**^{12d} and **L2c**^{12g} were reported by other groups while our groups had reported the crystal structure description of **L1d**, **L2d** and **L3c**¹¹. The following features were observed while analyzing the structural aspects of the compounds.

Crystal Structure Analysis of **L1a^{12b}:** The compound **L1a** had orthorhombic *Pbcn* space group and only half of the molecule was present in the asymmetric unit (Figure 1a). The molecules in **L1a** were packed in such a way that the N-N bonds of the adjacent molecules were arranged in parallel fashion with a distance of 3.810\AA between the two nitrogen of the neighboring molecules (Figure 1b). The aromatic moieties of the two adjacent molecules have inclined/tilted arrangements with centroid-to-centroid distance of 4.873\AA (Figure 1c). This results in a 1D arrangement of the molecules, which were further assembled in 3D via aromatic interactions between the inclined aromatic rings (centroid-to-centroid distance of 5.011\AA) (Figure 1c).

Crystal Structure Analysis of **L1b^{12c}:** The compound **L1b** was crystallized in monoclinic *P2₁/n* space group with one molecule present in the asymmetric unit. The molecule of **L1b** had a non planar geometry, where the C-N-N-C torsion angle was 138.72° and the two phenyl rings of a molecule were inclined at an angle of 64.62° (Figure 2a). Although inclined face-to-face stacking of the molecules were observed in this case due to the non planar geometry of the molecules, but the significant number of $\pi\cdots\pi$ interactions resulted in packing of the molecules (Figure 2c). The phenyl ring of a molecule of **L1b** was in the vicinity of neighboring phenyl rings such that the centroid-to-centroid distance between the aromatic rings was in the range of 4.6 - 4.9\AA (Figure 2b).

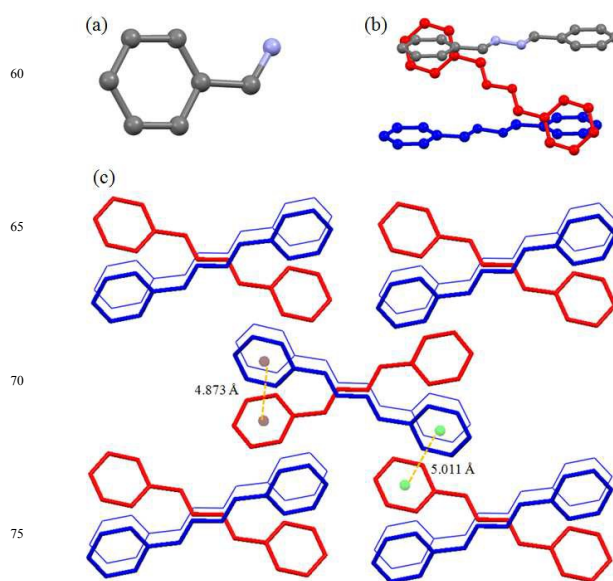


Figure 1: Illustration of Crystal Structure of **L1a**^{12b}: (a) Asymmetric Unit of **L1a**; (b) Arrangement of adjacent molecules; (c) Packing of the molecules (Figures were generated from the data obtained from CCDC No. 1118104)

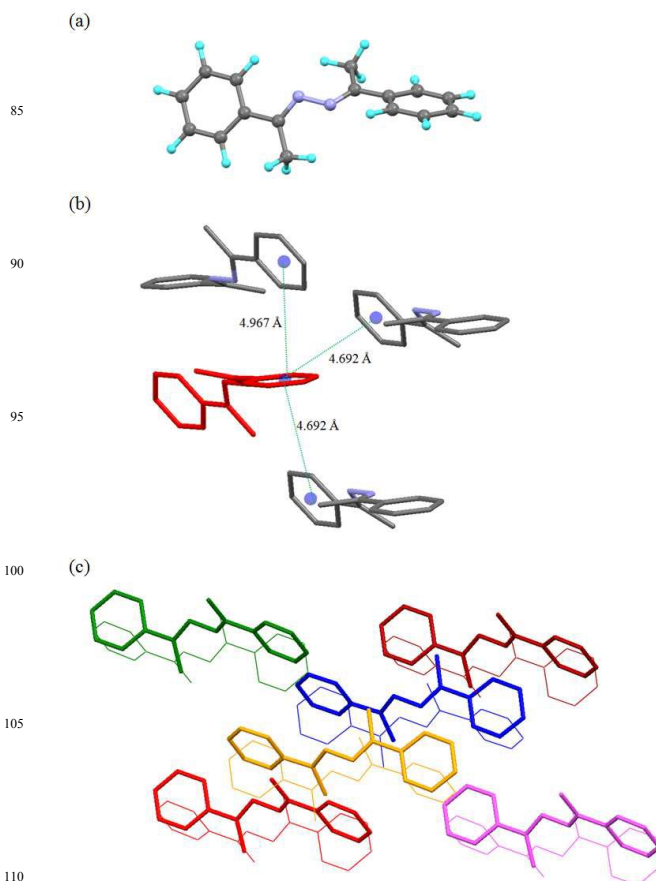


Figure 2: Illustration of Crystal Structure of **L1b**^{12c}: (a) Asymmetric Unit of **L1b**; Notice the non planar geometry of the molecule; (b) Centroid-to-Centroid distance between the adjacent aromatic rings; (c) Packing of the molecules (Figures were generated from the data obtained from CCDC No. 1207284)

Crystal Structure Analysis of L1d¹¹: The crystal structure analysis of **L1d** showed that there are three molecules in the asymmetric unit, which differed in the orientation of the pyridyl and imine moieties. The two molecules were arranged parallel such that they form dimer (Figure 3). The distance between the C=N of the two molecules were 3.906 and 3.943 Å, while the centroid to centroid distance between the two pyridyl rings were 3.888Å and 4.009Å. The third type of molecule interacted with the other two molecules *via* C-H...N and aromatic π ... π interactions and helped in the formation of dimers.

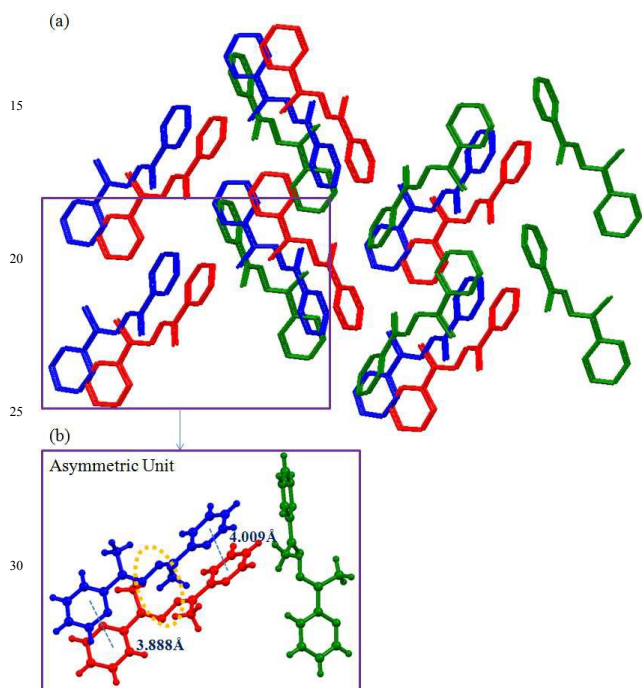


Figure 3: Illustration of Crystal Structure of **L1d¹¹**: (a) Packing of the molecules (Hydrogen atoms are removed for clarity); (b) Three types of molecules of **L1d** are present in the asymmetric unit, which are shown in different colors. (Figures were generated from the data obtained from CCDC No. 963345)

Crystal Structure Analysis of L2b^{12d}: The compound **L2b** was crystallized in $P2_1/n$ space group with half of the molecule in the asymmetric unit (Figure 4a). The ethyl group in the molecule adopted all *anti* conformation. The molecules were stacked in parallel manner to form a one-dimensional network (Figure 4b). The 3D arranged of the molecules can be viewed as herringbone arrangement of the one dimensional networks (Figure 4c).

Crystal Structure Analysis of L2d¹¹: The crystal structure of **L2d** was reported by our group¹¹ and it showed that there are two molecules in the asymmetric unit (Figure 5a). The ethyl spacer of **L2d** adopted *anti* conformation thereby resulting in linear geometry of the molecule. The neighboring molecules were arranged in a offset manner to form a one dimensional network (Figure 5b). The overall supramolecular network can be viewed as herringbone arrangement of these one dimensional network (Figure 5c).

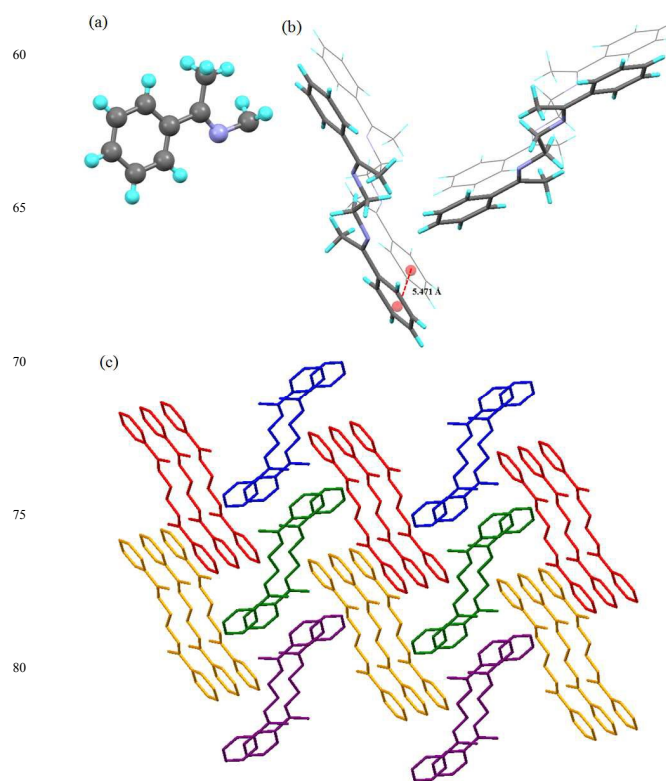


Figure 4: Illustration of Crystal Structure of **L2b^{12d}**: (a) Asymmetric Unit; (b) Arrangement of the molecules: Notice that the aromatic centroid-to-centroid distance is more than 5Å; (c) Herringbone arrangement of the molecules of **L2b** (Figures were generated from the data obtained from CCDC No. 608471)

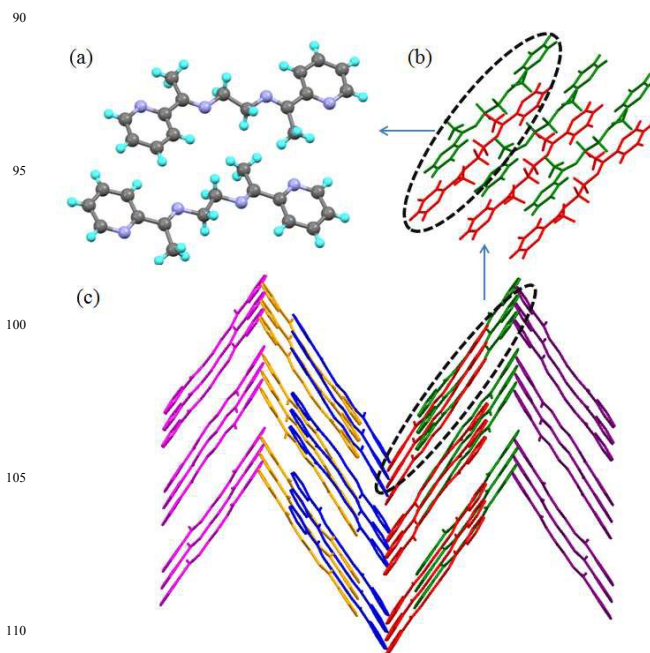


Figure 5: Illustration of Crystal Structure of **L2d¹¹**: (a) Asymmetric Unit; (b) Offset arrangement of the molecules to form 1D network; (c) Herringbone arrangement of the molecules of **L2d** (Hydrogen atoms were removed for clarity) (Figures were generated from the data obtained from CCDC No. 962823)

Crystal Structure Analysis of L2c^{12g} and L3c¹¹: The asymmetric unit in **L2c** has half of the molecule and the ethyl spacer adopts *gauche* conformation. The C-H...N hydrogen bond interactions between the pyridyl N and C-H of methinine resulted in the formation of "non-covalently bonded chromophore" unit (Figure 6a and 6b). The crystal structure analysis of **L3c** showed that it has half of the molecule in the asymmetric unit (Figure 6c). Further it was observed that the butyl spacer of **L3c** adopted *gauche-anti-gauche* conformation and not expected all *anti* conformation. The pyridyl-N...HC-(Methinine) interactions resulted in formation of a non covalently bonded "macrocyclic" moiety (Figure 6d). The butyl chain conformation resulted in formation of corrugated layers and offset packing of the layers results in the overall 3D arrangement of the **L3c** (Figure 6e).

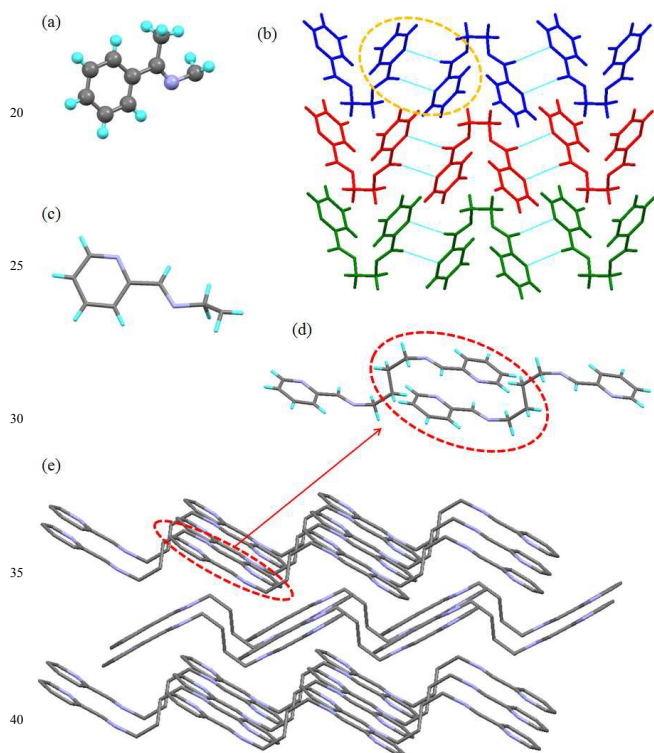


Figure 6: Illustration of Crystal Structure of **L2c^{12g}** and **L3c¹¹**: (a) Asymmetric unit in **L2c**; (b) Packing of the molecules of **L2c** via C-H...N interactions to form non covalent macrocyclic moiety; (c) Asymmetric Unit in **L3c**; (d) Non covalent "macrocyclic" moiety in **L3c**; (e) Offset packing of the corrugated layers in **L3c** (Hydrogen atoms are removed for clarity) (Figures were generated from the data obtained from CCDC No. 721559 (**L2c**) and 930055(**L3c**)).

Powder XRD Spectra of the compounds: Powder XRD spectra were recorded for **L1a**, **L1b**, **L2a**, **L2b**, **L3a**, **L3b**, **L4a** and **L4b**. The experimental powder XRD spectra of the compounds **L1a**, **L1b**, and **L2b** were compared with the simulated powder XRD spectra from the single crystal XRD data. Figure 7 shows the phase purity of the compounds **L1a**, **L1b**, and **L2b**. The

experimental spectra of other compounds are shown in Figure S25-S29.

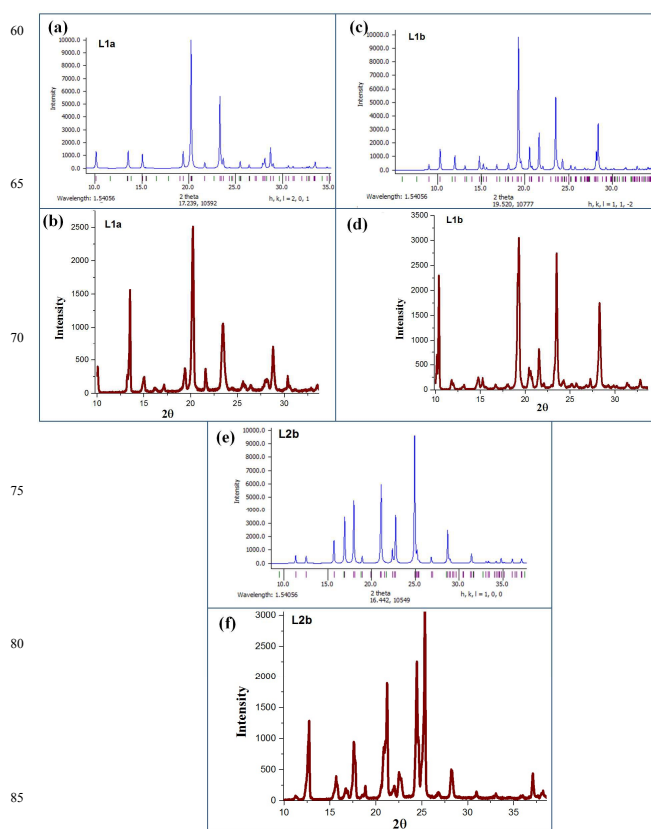


Figure 7: (a) Calculated XRD of **L1a**; Generated from Crystal Data CCDC No. 1118104; (b) Experimental XRD of **L1a**; (c) Calculated XRD of **L1b**; Generated from Crystal Data CCDC No. 1207284; (d) Experimental XRD of **L1b**; (e) Calculated XRD of **L2b**; Generated from Crystal Data CCDC No. 608471; (f) Experimental XRD of **L2b**

UV-Visible Absorption Spectra: The solid state UV-Visible spectra of **L1a** showed absorption maxima at 196nm ($\pi \rightarrow \pi^*$) and 300nm ($n \rightarrow \pi^*$) while **L1b** shows λ_{\max} at 206nm ($\pi \rightarrow \pi^*$) and 266nm ($n \rightarrow \pi^*$) (Figure 8a and 8b). The absorption maxima for **L1d¹¹** were at 253 nm ($\pi \rightarrow \pi^*$) and 286 nm ($n \rightarrow \pi^*$); which clearly indicated the effect of changing phenyl group with pyridyl group. The solid state UV-Visible absorption maxima for **L2a**, **L2b**, **L3a**, **L3b**, **L4a** and **L4b** were in the range 192-194 nm ($\pi \rightarrow \pi^*$) and 223-237 nm ($n \rightarrow \pi^*$) (Table 1, Figure 8c-8h), whereas for the **L2** and **L3** compounds with pyridyl group, the λ_{\max} was observed in the range of 232-235nm ($\pi \rightarrow \pi^*$) and 269-271 nm ($n \rightarrow \pi^*$)¹¹.

The UV-Visible absorption spectra in methanolic solution for the compounds **L1a**, **L1b**, **L2a**, **L2b**, **L3a**, **L3b**, **L4a** and **L4b** showed red shift (7-12nm) in the $\pi \rightarrow \pi^*$ peak position compared to their solid state spectra (Figure S30-S37); which indicates the possibility of parallel stacking of aromatic rings in solid state to form face-to-face stacking of the aromatic moieties/H-aggregates.¹³

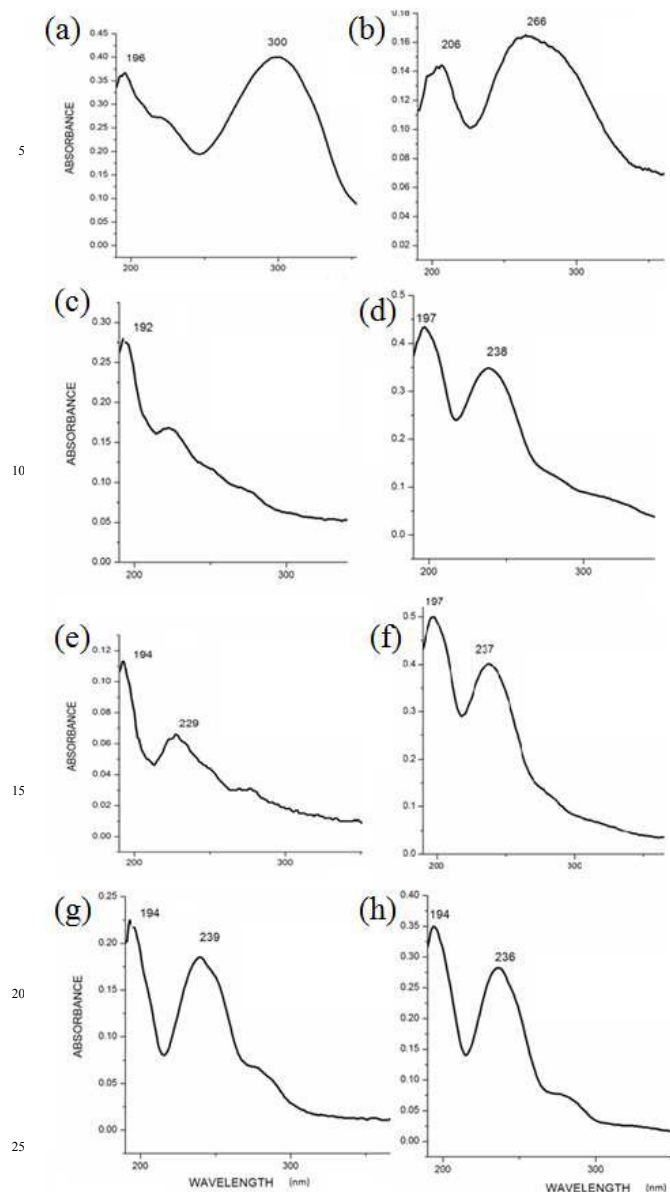


Figure 8: UV-Visible Absorption Spectra of compounds in Solid State (a) L1a; (b) L1b; (c) L2a; (d) L2b; (e) L3a; (f) L3b; (g) L4a; (h) L4b

Table 1: UV-Visible absorption maxima for compounds L1a, L1b, L2a, L2b, L3a, L3b, L4a and L4b

Compd	Solid State (λ_{\max} in nm)	Compds. in MeOH (conc. 10^{-4} M) (λ_{\max} in nm)
L1a	196, 300	206, 299
L1b	206, 266	205, 265
L2a	192, 223	209, 247
L2b	197, 238	207, 241
L3a	194, 229	204, 223
L3b	197, 237	205, 237
L4a	194, 239	203, 223
L4b	194, 236	206, 237

Photoluminescence Spectra of L2a and L2b: The PL spectra of L2a and L2b in solid state as well as in methanolic solutions showed the enhanced emission properties with increase in concentration. The observation from the concentration dependent PL spectra of L2a showed the appearance of a new peak on increasing concentration.

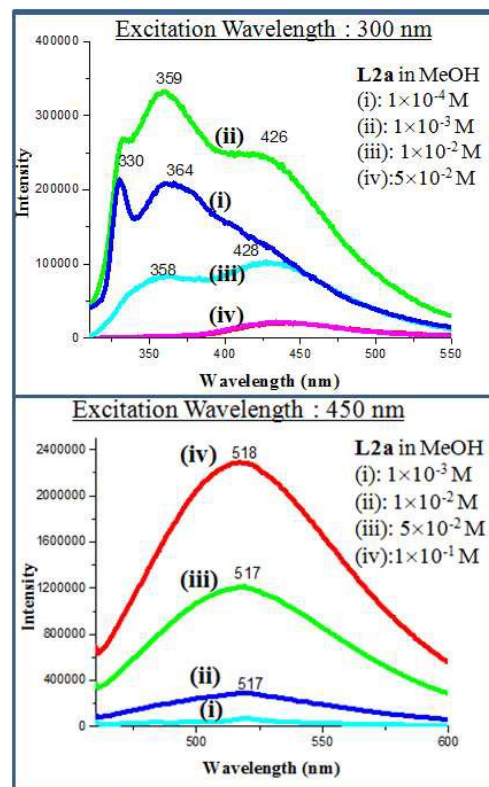


Figure 9: PL spectra of L2a in different concentrations

At 10^{-4} M concentration, by fixing the excitation wavelength at 300 nm, structured bands in PL spectra was observed with λ_{\max} at 330 and 364 nm, whereas at 10^{-3} M concentration, an extra shoulder peak appeared at 426 nm and at 5×10^{-1} M, band at around 359 nm disappeared completely and the only peak at 426 nm was observed. But when the excitation wavelength was fixed at 450 nm, concentration lower than 10^{-3} M didn't show any emission and on increasing the concentration to 10^{-1} M, an intense emission peak appeared at 518 nm (Figure 9). The PL spectra of L2b showed a structured emission spectra (λ_{\max} at 330 and 365 nm) at a concentration of 10^{-4} M, when the excitation wavelength was kept at 300 nm while a shoulder peak at 424 nm appeared at 10^{-3} M. On changing the excitation wavelength to 450 nm, 10^{-1} M concentration showed an intense peak at 500 nm (Figure 10). The PL spectra of L2c and L2d was reported previously by our group. In L2d, the PL spectra showed an increase in emission intensity along with a red shift of the peaks and the solid state PL showed a λ_{\max} at 453nm when excitation wavelength is at 400nm. The PL spectra of L2c showed the appearance of new peak on increasing concentration. It was suggested that the presence of pyridyl group resulted in C-H...N interaction and hence a non covalently bonded species appeared at high concentration.¹¹

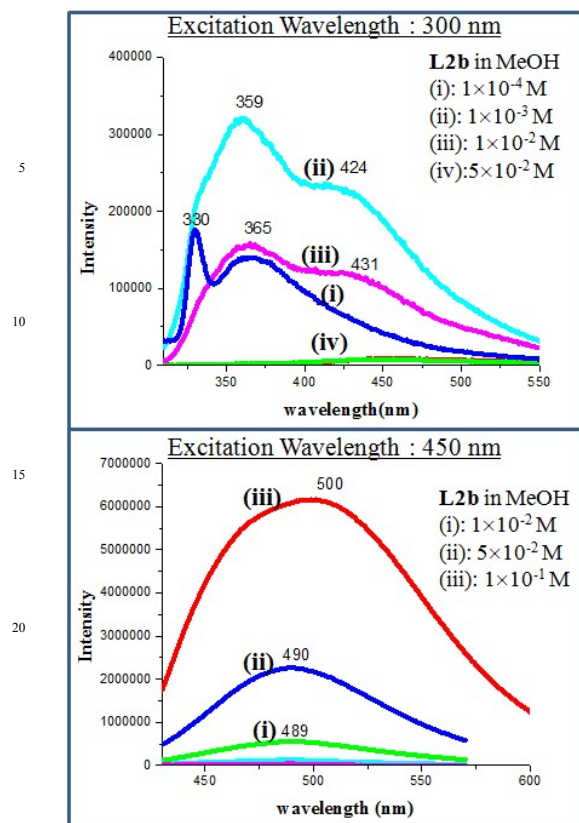


Figure 10: PL spectra of L2b in different concentrations

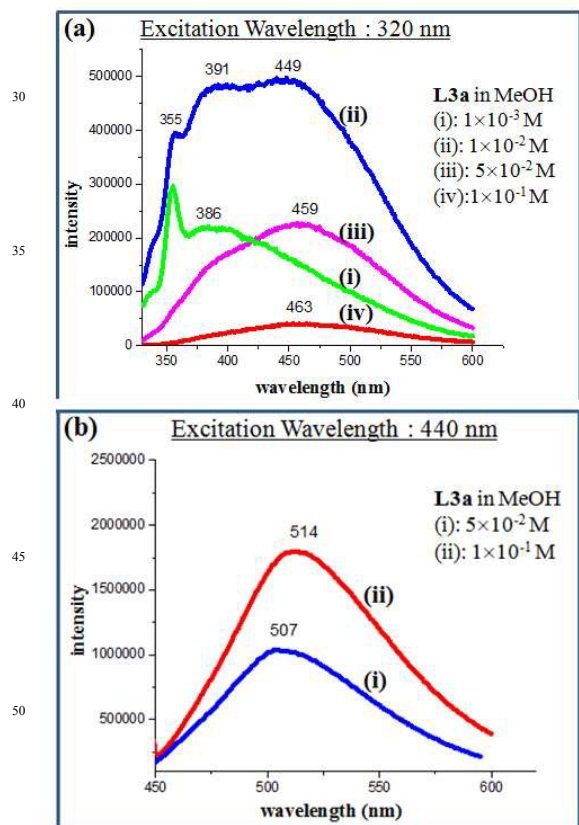


Figure 11: PL spectra of L3a in different concentrations

Photoluminescence Spectra of L3a, L3b, L4a and L4b: The PL spectra of L3a, L3b, L4a and L4b in methanolic solution also showed enhanced emission on increasing the concentration. The compound L3a showed a strong emission spectra at λ_{max} 514 nm (excitation wavelength at 440 nm) with a 10^{-1} M concentration, while L3b showed the emission maxima at 508 nm (excitation wavelength at 450 nm) with a 10^{-1} M concentration (Figure 11, 12 and S38). The compounds L4a and L4b at concentration of 10^{-1} M also showed emission maxima at 519 nm (excitation wavelength at 450 nm) and 420 nm (excitation wavelength at 493 nm), respectively (Figure S39). The PL spectra of L3c showed appearance of new peak at high concentration while L3d showed intensity increase along with red shift as reported previously by

70 us.

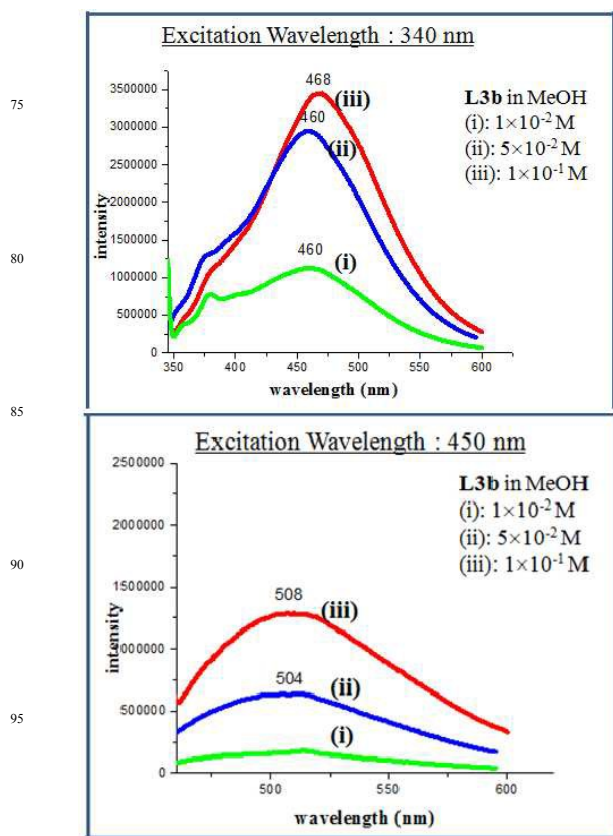


Figure 12: PL spectra of L3b in different concentrations

Solid State PL Spectra: The PL spectra of compounds L1a, L1b, L2a, L2b, L3a, L3b, L4a and L4b were recorded in their powder form and crystalline form to get a comparative analysis of the emissions in different states. Compounds L1a and L1b didn't show any PL spectra in powder as well as in crystalline state. The solid state PL of L2a showed an intense peak at 531 nm when the excitation wavelength was fixed at 350 nm, while L2b showed an intense peak at 549 nm. The solid state PL of L2a, L2b, L3a, L3b, L4a and L4b are shown in Figure S40-S44. Table 2 and table S1 shows the comparison of λ_{max} . For the compounds in solid state and in different concentrations in MeOH.

Concentration and Excitation Dependence of PL: The steady state PL measurements have shown that the emission of the compounds depends on concentration as well as excitation wavelength. On increasing concentration, at an excitation wavelength of around 300 nm, a red shift of emission maxima is observed along with the disappearance of peak in the region of 300nm (Table 2). Figure 13 shows the absorption and emission spectra of compound **L2a**. The absorption and emission wavelengths have very less overlap in the 300 nm range. Table 3 shows the molar extinction coefficients of UV-Vis spectra of **L2a** in wavelengths near 300nm. Although the molar extinction coefficient values are very less in the 300nm region, but reabsorption at higher concentration can be expected and to some extent may be reason for disappearance of peak at high concentration. Figure S45 and table S2 shows the overlap of absorption and emission spectra (at an excitation ~300 nm) and molar extinction coefficient of UV-Vis spectra in wavelength region 300nm, respectively of the compounds **L2b**, **L3a**, **L3b**, **L4a** and **L4b**.

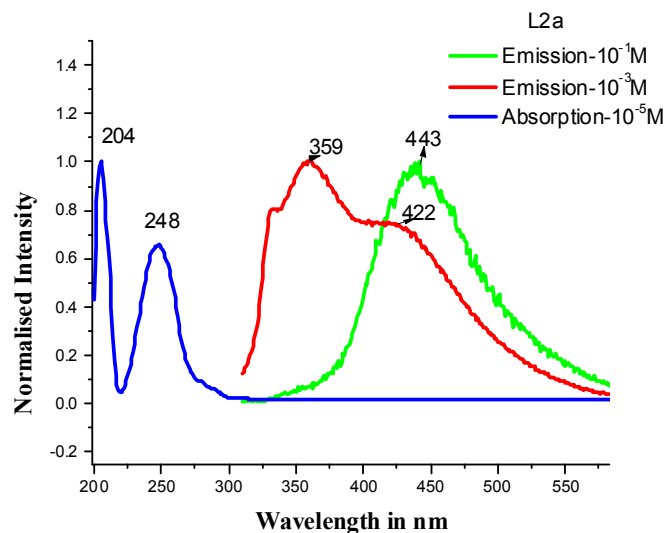


Figure 13: Absorption and emission spectra (excitation 300nm) of **L2a**

Table 2: λ_{max} in the PL Spectra of the compounds

	λ_{max} in Methanolic Solution of different concentration	λ_{max} in Solid
L2a	330, 364 (Excitation 300nm; $10^{-4}M$) 518 (Excitation 450 nm; $10^{-4}M$)	439 (Excitation 300nm; $10^{-1}M$) 518 (Excitation 450 nm; $10^{-1}M$)
L2b	330, 366 (Excitation 300nm; $10^{-4}M$) 489 (Excitation 450 nm; $10^{-4}M$)	464 (Excitation 300nm; $10^{-1}M$) 500 (Excitation 450 nm; $10^{-1}M$)
L3a	365, 386 (Excitation 320nm; $10^{-3}M$) 479 (Excitation 420 nm; $10^{-4}M$)	463 (Excitation 320 nm; $10^{-1}M$) 509 (Excitation 420 nm; $10^{-1}M$)
L3b	376, 460 (Excitation 340nm; $10^{-2}M$) 478 (Excitation 420nm; $10^{-4}M$)	382 (Excitation 320 nm; $10^{-1}M$) 504 (Excitation 450 nm; $10^{-2}M$)
L4a	300, 370 (Excitation 280nm; $10^{-4}M$) 517 (Excitation 450 nm; $10^{-4}M$)	514 (Excitation 280 nm; $10^{-1}M$) 517 (Excitation 450 nm; $10^{-2}M$)
L4b	350, 420 (Excitation 320nm; $10^{-3}M$) 484 (Excitation 420 nm; $10^{-4}M$)	465 (Excitation 320 nm; $10^{-1}M$) 490 (Excitation 420 nm; $10^{-2}M$)

Further, the dependence of emission wavelength on the excitation wavelength is observed from table 2 and table S1. The dependence is more pronounced at lower concentration. In **L2a**, at $10^{-4}M$ concentration, emission maxima are observed at 330nm, 364 nm (when the excitation wavelength is 300nm) while emission maxima is observed at 518 nm (when the excitation wavelength is 450 nm). This dependence clearly shows the formation of aggregate species, which are responsible for different emission peaks at different excitation.

Table 3: Molar Extinction Coefficient of UV-Vis spectra of **L2a** in wavelengths near 300nm

Compounds	Molar coefficient (ϵ) ($M^{-1}cm^{-1}$)	Wavelength in nm		
L2a	$10^{-3}M$	195.2 330		
	$10^{-4}M$	829 1095 3533 4793	330 300 289 280	
		$10^{-5}M$	3190 4510 7970 10610 61690 91310	330 300 289 280 248 205

Time-Resolved Fluorescence Technique for Lifetime Analysis:

With the help of the time-correlated single-photon counting (TCSPC) technique, we have measured the excited-state decay curve of the compounds (Figure S46-S51). The compounds showed a tri-exponential decay, with three lifetimes in the range of 1-2 ns, 4-7ns and 0.1 -0.2 ns at concentration more than $10^{-4}M$. The shortest lifetime may be attributed to the deactivation (quenching) of excited aromatic groups while the longer lifetime is associated with the unquenched decay of the compounds. Table 4 and Table S3 summarize the lifetime measurements of the compounds.

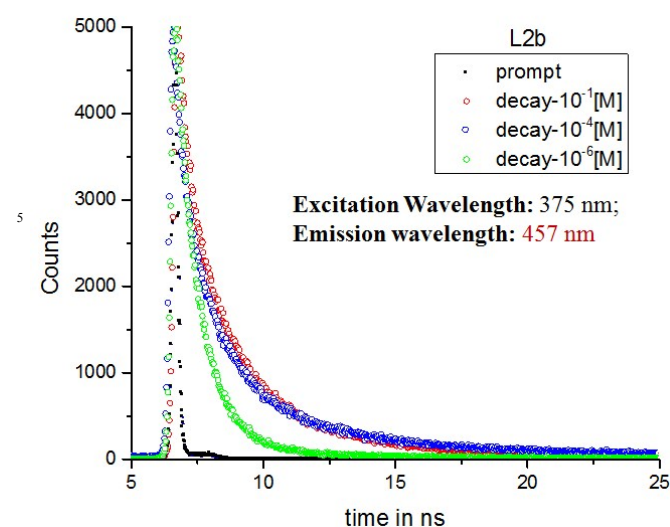


Figure 14: TCSPC decay profiles of **L2b** in different concentration in MeOH with excitation at 375 nm

Table 4: Fluorescence lifetime data for **L2a**, **L2b**, **L3a**, **L3b**, **L4a** and **4b**

$\lambda_{\text{Excitation}} = 375\text{nm}$	τ_1 (ns)	τ_2 (ns)	τ_3 (ns)	τ_{avg} (ns)
L2a 10^{-1} $\lambda_{\text{Emission}} 520\text{ nm}$	1.55 (α_1 0.30)	5.66 (α_2 0.10)	0.23 (α_3 0.60)	1.153 (χ^2 1.24)
10^{-4} $\lambda_{\text{Emission}} 449\text{ nm}$	1.23 (α_1 0.35)	0.26 (α_2 0.54)	4.69 (α_3 0.11)	1.076 (χ^2 1.05)
L2b 10^{-1} $\lambda_{\text{Emission}} 457\text{nm}$	1.48 (α_1 0.38)	4.17 (α_2 0.13)	0.23 (α_3 0.49)	1.209 (χ^2 1.15)
10^{-4} $\lambda_{\text{Emission}} 457\text{nm}$	1.51 (α_1 0.37)	5.92 (α_2 0.08)	0.21 (α_3 0.55)	1.172 (χ^2 1.11)
10^{-6} $\lambda_{\text{Emission}} 457\text{nm}$	0.79 (α_1 0.97)	4.56 (α_2 0.03)	--	0.90 (χ^2 1.40)
L3a 10^{-1} $\lambda_{\text{Emission}} 500\text{nm}$	1.39 (α_1 0.21)	5.43 (α_2 0.11)	0.17 (α_3 0.0.68)	1.00 (χ^2 1.23)
10^{-2} $\lambda_{\text{Emission}} 463\text{nm}$	0.99 (α_1 0.19)	4.53 (α_2 0.09)	0.12 (α_3 0.72)	0.682 (χ^2 1.11)
L3b 10^{-1} $\lambda_{\text{Emission}} 477\text{nm}$	2.50 (α_1 0.19)	7.43 (α_2 0.24)	0.24 (α_3 0.57)	2.416 (χ^2 1.14)
10^{-5} $\lambda_{\text{Emission}} 473\text{nm}$	6.24 (α_1 0.93)	4.83 (α_2 0.07)	-	0.903 (χ^2 1.34)
L4a 10^{-1} $\lambda_{\text{Emission}} 464\text{nm}$	1.93 (α_1 0.17)	6.90 (α_2 0.11)	0.15 (α_3 0.72)	1.201 (χ^2 1.20)
10^{-4} $\lambda_{\text{Emission}} 460\text{nm}$	0.86 (α_1 0.43)	5.29 (α_2 0.11)	0.19 (α_3 0.46)	1.021 (χ^2 1.21)

L4b 10^{-1} $\lambda_{\text{Emission}} 540\text{nm}$	1.42 (α_1 0.11)	5.52 (α_2 0.37)	0.19 (α_3 0.52)	2.29 (χ^2 1.18)
10^{-2} $\lambda_{\text{Emission}} 530\text{nm}$	1.56 (α_1 0.09)	6.02 (α_2 0.36)	0.17 (α_2 0.36)	2.39 (χ^2 1.29)

Methanolic solution of **L2b** of concentrations 10^{-1} M, and 10^{-4} M showed a tri exponential decay when excited at 375 nm and emission was monitored at 457 nm, while a bi exponential decay was observed at a concentration of 10^{-6} M. The average lifetime of 10^{-1} M was 1.209 ns, 10^{-4} was 1.17 and 10^{-6} M was 0.90 ns (Figure 14). The concentration dependence of the TCSPC profile of the **L2b** suggested the aggregation of the molecules at higher concentration. The increase in the average lifetime with concentration suggests that with aggregation in concentrated solution, the unquenched decay processes increases, which may be considered to be aggregation induced emission.

Fluorescence Quantum Yield: Fluorescence quantum yield was determined for the compounds **L2a**, **L2b**, **L3a**, **L3b**, **L4a** and **L4b** in spectroscopic grade methanol using optically matching solutions of quinine sulfate ($\Phi_f = 0.546$ in 0.5 H_2SO_4 at an excitation wavelength of 345 nm) as standard. In solid state, sample was mixed with BaSO_4 to measure the absolute quantum yield.

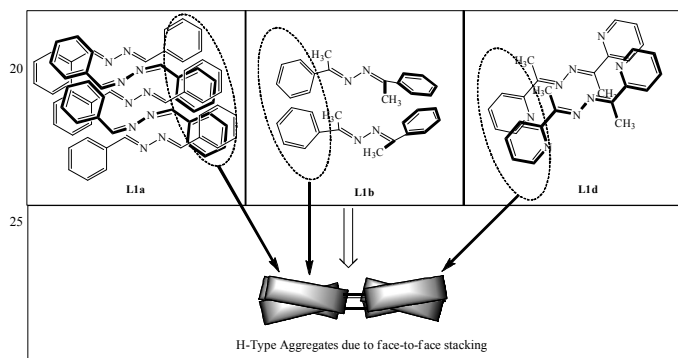
Table 5: Absolute Quantum Yield in solution and in solid

Compd.	10^{-1}			Compd.	10^{-4} 10^{-1}		
	10^{-4} M	M	Solid		M	M	Solid
L2a (Φ_f)	1.06	4.04	5.81	L2b (Φ_f)	0.89	1.52	2.28
Excitation (nm)	300	450	350	Excitation (nm)	300	450	350
Emission (nm)	365	515	530	Emission (nm)	365	515	545
L3a (Φ_f)	1.24	5.48	13.57	L3b (Φ_f)	1.09	2.68	9.98
Excitation (nm)	320	440	440	Excitation (nm)	320	450	420
Emission (nm)	380	505	524	Emission (nm)	390	505	492
L4a (Φ_f)	1.98	7.58	18.68	L4b (Φ_f)	1.32	4.48	14.46
Excitation (nm)	340	450	450	Excitation (nm)	340	420	460
Emission (nm)	370	515	515	Emission (nm)	370	490	530

It was observed that the quantum yield of the compounds in dilute solution (10^{-4} M in MeOH) was in the range of 0.89-1.98, while on increasing the concentration to 10^{-1} M, Φ_f were observed in range of 1.52-7.58. The absolute quantum yield in solid state showed a further increase and values were in the range 2.28-

18.68. An interesting trend was observed in the quantum yield for these compounds (Table 5). The compounds **L2a**, **L3a** and **L4a** showed a higher quantum yield than that of **L2b**, **L3b** and **L4b**, respectively. Further, on increasing the alkyl spacer length, the quantum yield was observed to increase.

Correlating the Enhanced Emission of the compounds with their Crystal Structure: The absence of fluorescence in **L1a**, **L1b**, **L1c** and **L1d** can be explained by observing their crystal structures. In the solid state of **L1a**, the molecule has planar geometry. The aromatic rings of the neighboring molecules are tilted and inclined face-to-face stacking is observed. The UV-Visible absorption maxima of crystalline/solid **L1a** showed a blue shift compared to that in MeOH (10^{-4} M). Both the crystal structure as well as the absorption spectra indicated that in **L1a**, the formation of H-aggregates in the solid state and in concentrated solution, which may be attributed to the absence of fluorescence.



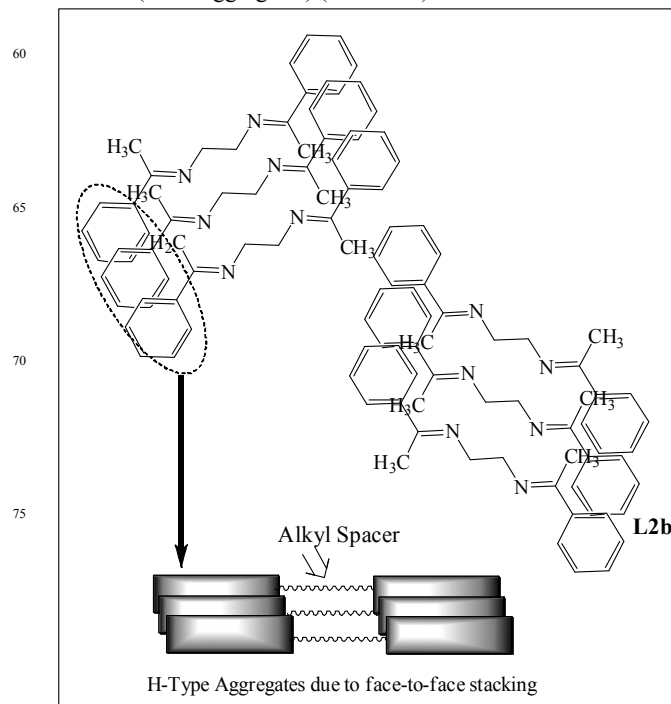
Scheme 2: Arrangement of the molecules of **L1a**, **L1b** and **L1d** in the solid state; Notice the face-to-face stacking of the molecules. Although it is inclined in case of **L1a** and **L1b**, no fluorescence is observed in solid state

In **L1b**, the non planar geometry of the molecule along with face-to-face stacking of the molecules has resulted in quenching of fluorescence, while in **L1d**, quenching of fluorescence is explained by the dimer formation in the solid state (Scheme 2).

Although the crystal structure of **L1c** is not reported, we can speculate that non radiative decay due to the head-to-head arrangement of the molecules.

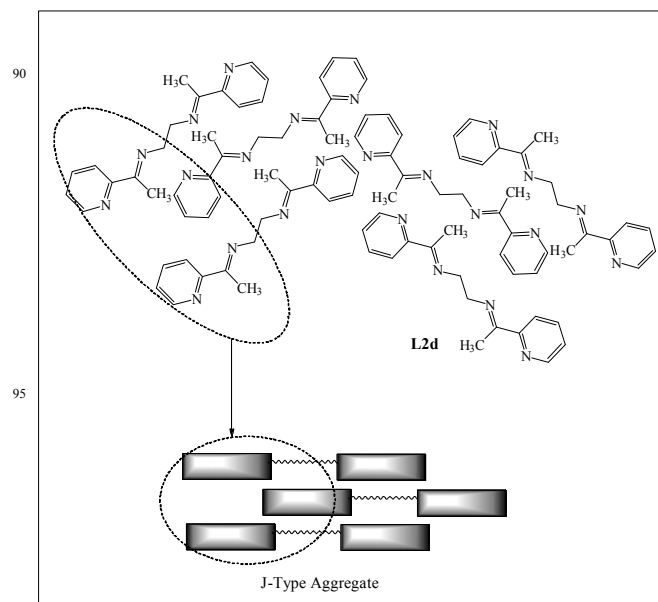
In **L2b**, the molecules attain planarity in the solid state and face-to-face stacking of the molecules is observed. This is similar to the formation of H-aggregates, which is defined as the parallel alignment of the molecules and blue shifted absorption bands. The blue shifted UV-Visible bands (about 8 nm) and the crystal structure of **L2b** shows that they form H-aggregates. The appearance of the new peak in the PL spectra at higher concentration and red shift of that peak indicates that a new emissive species has formed in the high concentration. The crystal structure analysis shows that although H-aggregates are formed in **L2b**, these aggregates are reason for its high emission properties. The crystal structures of **L2c**, **L3a**, **L3b**, **L4a** and **L4b** are not reported, but the similar trend in UV-Visible absorption spectra and PL spectra indicates that the solid state arrangement of the

molecules may involve parallel face-to-face stacking of the molecules (or H-Aggregates) (Scheme 3).



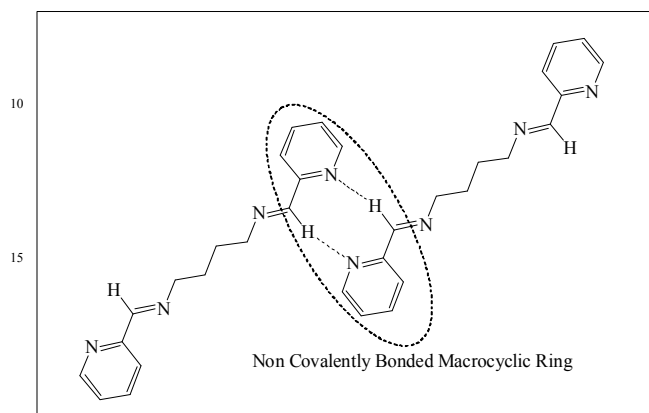
Scheme 3: Arrangement of the molecules of **L2b**; **L2a**, **L3a**, **L3b**, **L4a** and **L4b** are also expected to have similar arrangements in the solid state. Notice the face-to-face stacking of the molecules

In **L2d**, the attainment of the planar geometry and offset arrangement of molecules resulted in increased emission in PL spectra on increasing concentration and in the solid state and similar behavior is expected for **L3d** in solid state (Scheme 4).



Scheme 4: Arrangement of the molecules of **L2d** and **L3d** in the solid state; Notice the offset stacking of molecules

In **L2c** and **L3c**, it was reported previously by our group, that the formation of a new "chromophore" species at concentration and in solid state resulted in increased emission spectra. The crystal structure analysis of **L3c** showed that the non covalent interactions led to the arrangement of the molecules in "non covalently bonded macrocyclic rings" (Scheme 5).



Scheme 5: Arrangement of the molecules of **L2c** and **L3c** in the solid state; Notice the formation of new "Chromophore" on aggregation and in the solid state

NMR Assay to Detect the Aggregation in Concentrated Solution: The effect of changing the concentration on the NMR spectra of aggregating compounds include changes in the chemical shifts, shape and intensity of the peaks on changing the concentration.¹⁴ The ¹H-NMR of compounds **L1a**, **L1b**, **L2b** and **L3b** were recorded in different concentrations in CDCl₃. The indication of the possible molecular arrangement on aggregation/in concentrated solution may be obtained from final arrangement of the molecules in the solid state.

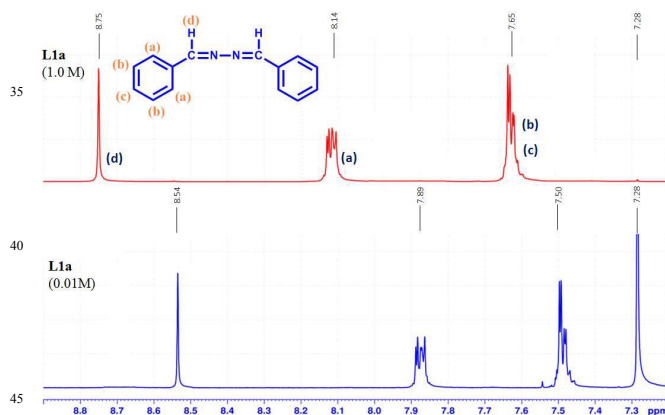


Figure 15: ¹H NMR spectra of **L1a** in different concentrations in CDCl₃

The concentration dependent ¹H-NMR of **L1a** showed that the aromatic protons and the methine protons resonated in deshielded region when the concentration was increased from 0.01M to 1M (Figure 15). The aggregation of molecules at higher concentration has resulted in the change in chemical of the

protons. From the crystal structure analysis of **L1a**, it was observed that the molecules have tilted face-to-face arrangement and the aromatic moieties are clustered together.

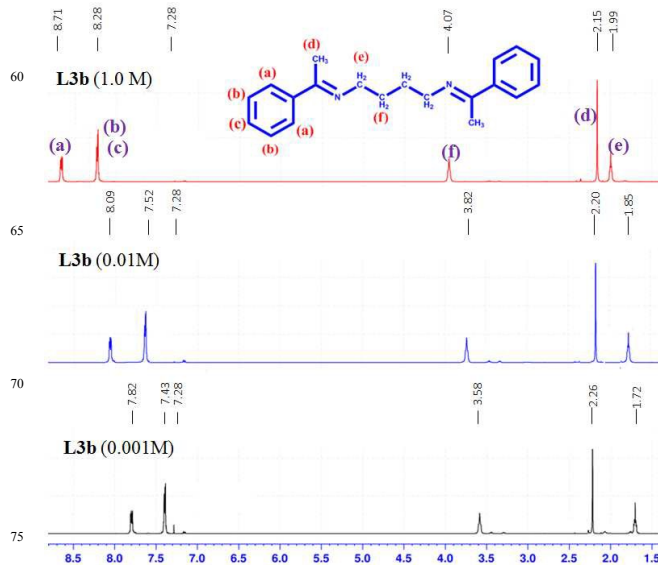
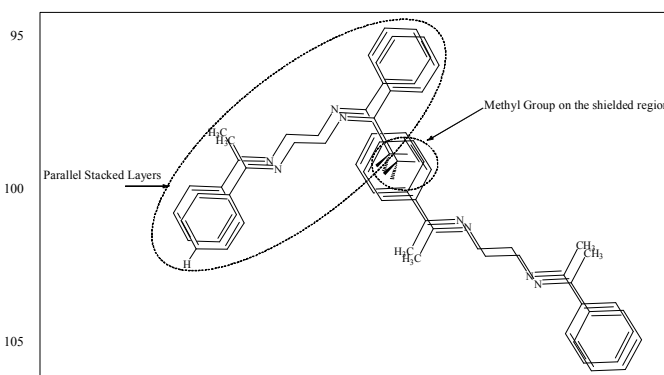


Figure 16: ¹H NMR spectra of **L3b** in different concentrations in CDCl₃

The concentration dependent ¹H NMR spectra of **L2b** and **L3b** was recorded in CDCl₃ (Figure 16, Figure S52). In both the cases, it was observed that the protons in the aromatic region resonated in the deshielded region when the concentration was increased from 10⁻² M to 1M, whereas the methyl protons resonated in the shielded region on increasing the concentration. The crystal structure analysis of **L2b** showed the parallel stacking of the aromatic rings, which may be associated with the deshielding effects of aromatic protons on increasing concentrations, while on closely observing the structure, it was seen that the herringbone arrangement of the parallel stacked layer resulted in positioning of the methyl groups in such a way that they fall just above the aromatic rings (Scheme 6), which explains the shielding effect of the methyl protons on increasing concentration.



Scheme 6: Arrangement of the molecules in **L2b** and **L3b** resulted in deshielded aromatic proton and shielded methyl protons

The concentration dependent $^1\text{H-NMR}$ of **L2d** in CDCl_3 showed that the increase in concentration from 10^{-2} M to 1M resulted the aromatic proton to resonate in shielded region (Figure 17, Figure S53). The shielded aromatic proton in concentration solutions of **L2d** may be due to the offset arrangement of the molecules. So face-to-face stacking of aromatic rings are absent in **L2d**, which in case of **L1a**, **L2b** and **L3b** has resulted in deshielding effects.

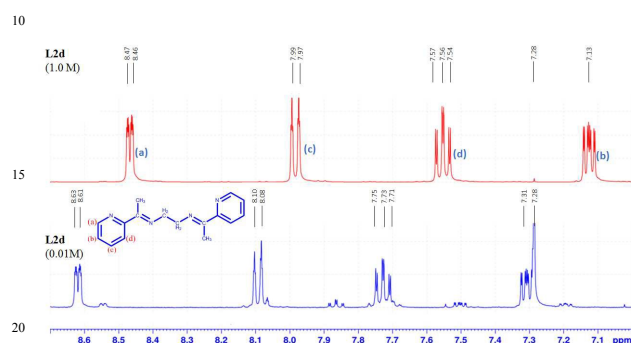


Figure 17: ^1H NMR spectra of **L2d** in different concentrations in CDCl_3

The NOESY of **L2b** at 2M concentration in CDCl_3 was taken to observe the interaction between different types of protons at higher concentration due to aggregation. The spectrum showed interaction between the aromatic protons 'a' and aromatic protons 'b', 'c' & between aromatic protons ('a', 'b', 'c') and the methyl proton ('d') (Figure 18). This suggested that at high concentration, the methyl protons interact with the aromatic protons and a structure similar to scheme 6 may be possible. Further the interaction between the aromatic protons also suggest a face-to-face stacking of the molecules at higher concentration.

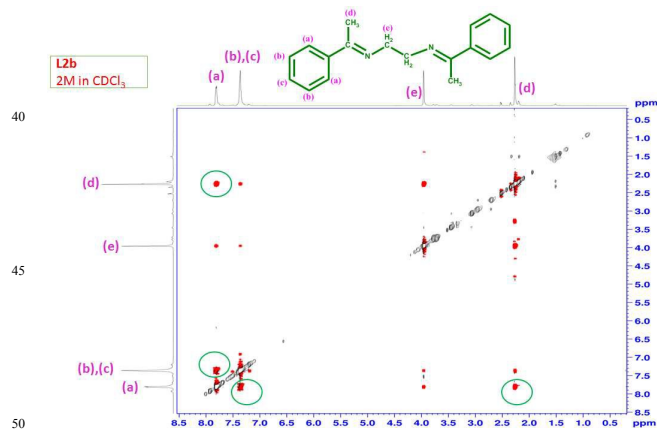


Figure 18: NOESY of **L2b** in CDCl_3 at a concentration of 2M

Conclusions

Systematic study of unique AIE properties of di Schiff base compounds were carried out. The crystal structure analysis of

some of these compounds have given us the idea about interplay of non covalent interactions and crystal packing on the photo physical properties of the compounds. Apart from the compounds with hydrazine spacer i.e. **L1**, all the other compounds have small π -conjugated systems linked with alkyl spacers. In **L1**, where extended conjugation is present throughout the molecule didn't show any fluorescence, while other compounds with alkyl spacer show good emission properties. The emission properties of these compounds are related to the arrangement of the molecules in aggregated states. In **L1**, the H-aggregate formation/ dimer formation resulted in quenching of fluorescence. In **L2b**, the H-aggregate formation was evident from crystal structure and UV-Visible absorption spectra, but AIE properties were observed. The alkyl spacer in **L2b** is preventing the non-radiative decay processes usually observed for H-aggregated. The compounds **L2a**, **L3a**, **L3b**, **L4a** and **L4b** were also expected to show similar packing as that of **L2b** and the enhanced emission properties of these compounds are attributed to the presence of the alkyl spacers.

Acknowledgement

We gratefully acknowledge the financial support from DST (SR/FT/CS-24/2011) and Instrumentation facility from the DST FIST & UGC-SAP to the Department of Chemistry, BITS Pilani, Pilani Campus. We also acknowledge the DST FIST supported Powder XRD facility of the Department of Physics, BITS Pilani, Pilani Campus.

Notes and references

- Department of Chemistry, Birla Institute of Technology and Science, Pilani, Pilani Campus, Rajasthan, India. Fax: +91-1596-244183; Tel: +91-1596-515679; E-mail: msarkar@pilani.bits-pilani.ac.in
- † Electronic Supplementary Information (ESI) available: [IR, ^1H NMR, ^{13}C NMR, UV absorption spectra, Photo Luminescence Spectra and other supplementary material.]. See DOI: 10.1039/b000000x/
- ‡ Footnotes should appear here. These might include comments relevant to but not central to the matter under discussion, limited experimental and spectral data, and crystallographic data.
1. (a) T. W. Kelley, P. F. Baude, C. Gerlach, D. E. Ender, D. Muires, M. A. Haase, D. E. Vogel and S. D. Theiss, *Chem. Mater.* **2004**, *16*, 4413; (b) C-T. Chen, *Chem. Mater.* **2004**, *16*, 4389; (c) H. Yersin, Highly Efficient OLEDs with Phosphorescent Materials, Wiley-VCH, Weinheim, **2008**; (d) H. N. Kim, Z. Q. Guo, W. H. Zhu, J. Yoon and H. Tian, *Chem. Soc. Rev.*, **2011**, *40*, 79; (e) J. S. Wu, W. M. Liu, J. C. Ge, H. Y. Zhang and P. F. Wang, *Chem. Soc. Rev.*, **2011**, *40*, 3483; (f) Y. Tao, C. Yang and J. Qin, *Chem. Soc. Rev.*, **2011**, *40*, 2943; (g) H. Sasabe and J. Kido, *Chem. Mater.* **2011**, *23*, 621; (h) M. Schaferling, *Angew. Chem., Int. Ed.*, **2012**, *51*, 3532; (i) M. Zhu and C. Yang, *Chem. Soc. Rev.*, **2013**, *42*, 4963; (j) A. M. Breul, M. D. Hager and U. S. Schubert, *Chem. Soc. Rev.*, **2013**, *42*, 5366.
- (a) J. Luo, Z. Xie, J. W. Y. Lam, L. Cheng, H. Chen, C. Qiu, H. S. Kwok, X. Zhan, Y. Liu, D. Zhu and B. Z. Tang, *Chem. Commun.*, **2001**, 1740; (b) B. Z. Tang, X. Zhan, G. Yu, P. P. S. Lee, Y. Liu and D. Zhu, *J. Mater. Chem.*, **2001**, *11*, 2974; (c) Y. Hong, J. W. Y. Lam and B. Z. Tang, *Chem. Soc. Rev.*, **2011**, *40*, 5361; (d) R. Hu, N. L. C. Leung and B. Z. Tang, *Chem. Soc. Rev.*, **2014**, *43*, 4494.
- (a) B. K. An, S. K. Kwon, S. D. Jung and S. Y. Park, *J. Am. Chem. Soc.*, **2002**, *124*, 14410; (b) S. Y. Ryu, S. Kim, J. Seo, Y. W. Kim, O. H. Kwon, D. J. Jang and S. Y. Park, *Chem. Commun.*, **2004**, 70; (c) Y. You, H. S. Huh, K. S. Kim, S. W. Lee, D. Kim and S. Y. Park, *Chem. Commun.*, **2008**, 3998; (d) B. K. An, S. H. Gihm, J. W. Chung, C. R. Park, S. K. Kwon and S. Y. Park, *J. Am. Chem. Soc.*, **2009**, *131*, 3950; (e) J. W. Chung, B. K. An and S. Y. Park, *Chem. Mater.*, **2008**, *20*, 6750.

4. (a) Z. J. Ning, Z. Chen, Q. Zhang, Y. L. Yan, S. X. Qian, Y. Cao and H. Tian, *Adv. Funct. Mater.*, **2007**, *17*, 3799; (b) Z. Ning and H. Tian, *Chem. Commun.*, **2009**, 5483; (c) B. Wang, Y. C. Wang, J. L. Hua, Y. H. Jiang, J. H. Huang, S. X. Qian and H. Tian, *Chem.–Eur. J.*, **2011**, *17*, 2647.
5. (a) Y. Hong, J. W. Y. Lama and B. Z. Tang, *Chem. Commun.*, **2009**, 4332; (b) M. Levitus, K. Schmieder, H. Ricks, K. D. Shimizu, U. H. F. Bunz and M. A. Garcia-Garibay, *J. Am. Chem. Soc.*, **2001**, *123*, 4259.
6. (a) S. P. Anthony, S. Varughese and S. M. Draper, *J. Phys. Org. Chem.*, **2010**, *23*, 1074; (b) S. P. Anthony, S. Varughese and S. M. Draper, *Chem. Commun.*, **2009**, 7500.
7. S. Varughese, *J. Mater. Chem. C*, **2014**, *2*, 3499.
8. (a) E. Hadjoudis and I. M. Mavridis, *Chem. Soc. Rev.*, **2004**, *33*, 579; (b) P. G. Cozz, *Chem. Soc. Rev.*, **2004**, *33*, 410; (c) M. Andruh, *Chem. Commun.*, **2011**, *47*, 3025.
9. T. Kawasaki, T. Kamata, H. Ushijima, S. Murata, F. Mizukami, Y. Fujii and Y. Usui, *Mol. Cryst. Liq. Cryst.*, **1996**, *286*, 257.
10. (a) W. Tang, Y. Xiang and A. Tong, *J. Org. Chem.*, **2009**, *74*, 2163; (b) R. Wei, P. Song and A. Tong, *J. Phys. Chem. C*, **2013**, *117*, 3467; (c) X. Chen and A. Tong, *J. Lumin.*, **2014**, *145*, 737; (d) X. F. Ma, J. H. Cheng, J. Y. Liu, X. G. Zhou and H. F. Xiang, *New J. Chem.*, **2015**, *39*, 492; (e) J. Cheng, Y. Li, R. Sun, J. Liu, F. Gou, X. Zhou, H. Xiang and J. Liu, *J. Mater. Chem. C*, **2015**, *3*, 11099.
11. F. Baig, Rajnikant, V. K. Gupta and M. Sarkar, *RSC Adv.*, **2015**, *5*, 51220.
12. (a) L. N. Ferguson, T. C. Goodwin, *J. Am. Chem. Soc.*, **1949**, *71*, 633; (b) U. C. Sinha, *Acta Cryst., B*, **1970**, *26*, 889; (c) G. S. Chen, M. Anthamatten, C. L. Barnes, and R. Glaser, *J. Org. Chem.*, **1994**, *59*, 4336; (d) R. E. Benson, T. G. Roy, B. K. Dey, K. K. Barua and E. R. T. Tiekink, *Acta Cryst. E*, **2006**, *62*, o1971; (e) V. A. Sauro and M. S. Workentin, *J. Org. Chem.*, **2001**, *66*, 831; (f) X. D. Tang, Z. J. Ding and Z. M. Zhang, *Solid State Comm.*, **2009**, *149*, 301; (g) A. K. El-Qisairi, H. A. Qaseer, S. F. Alshahateet, M. K. H. Qaseer, M. H. Zaghal, W. Al-Btoush, and L. N. Dawed, *Croat. Chem. Acta*, **2014**, *87*, 123.
13. (a) L. Wang, Y. Shen, M. Yang, X. Zhang, W. Xu, Q. Zhu, J. Wu, Y. Tiana and H. Zhou, *Chem. Commun.*, **2014**, *50*, 8723; (b) S. Basak, N. Nandi, A. Baral and A. Banerjee, *Chem. Commun.*, **2015**, *51*, 780.
14. (a) A. Mitra, P. J. Seaton, R. A. Assarpour and T. Williamson, *Tetrahedron*, **1998**, *54*, 15489; (b) S. R. LaPlante, R. Carson, J. Gillard, N. Aubry, R. Coulombe, S. Bordeleau, P. Bonneau, M. Little, J. O'Meara and P. L. Beaulieu, *J. Med. Chem.*, **2013**, *56*, 5142.

Photo Physical Properties of Di-Schiff Bases: Evaluating the Synergistic Effect of Non Covalent Interactions and Alkyl Spacer in Enhanced Emissions of Solids

Moyna Das, Fayaz Baig and Madhushree Sarkar*

The di-Schiff bases with alkyl spacer (ethyl, butyl and hexyl) showed enhanced light emitting properties in solid state, while quenching was observed for di-Schiff bases with hydrazine spacer. The crystal structure analysis of the compounds showed that the packing of the molecules *via* non covalent interactions along with the flexible spacer played the role in dictating the emission properties.

